

Heterogeneous & Homogeneous & Bio- & Nano-

# CHEMCATCHEM

CATALYSIS

## Accepted Article

**Title:** Electroactivity of Urea Oxidation on NiCr Catalysts in Alkaline Electrolyte

**Authors:** Ramesh Kumar Singh and Alex Schechter

This manuscript has been accepted after peer review and appears as an Accepted Article online prior to editing, proofing, and formal publication of the final Version of Record (VoR). This work is currently citable by using the Digital Object Identifier (DOI) given below. The VoR will be published online in Early View as soon as possible and may be different to this Accepted Article as a result of editing. Readers should obtain the VoR from the journal website shown below when it is published to ensure accuracy of information. The authors are responsible for the content of this Accepted Article.

**To be cited as:** *ChemCatChem* 10.1002/cctc.201700451

**Link to VoR:** <http://dx.doi.org/10.1002/cctc.201700451>

WILEY-VCH

[www.chemcatchem.org](http://www.chemcatchem.org)



# Electroactivity of Urea Oxidation on NiCr Catalysts in Alkaline Electrolyte

Ramesh Kumar Singh<sup>[a]</sup> and Alex Schechter<sup>\*[b]</sup>

**Abstract:** Inexpensive Ni-based catalysts have shown comparable urea oxidation activity to that of precious metals in an alkaline electrolyte. We investigated urea oxidation on binary NiCr supported on a carbon matrix in 1 M KOH and 0.33 M urea. The amount of Cr is optimized in the catalyst layer and it was found that catalyst with 40% Cr (Ni<sub>60</sub>Cr<sub>40</sub>/C) exhibits the highest urea oxidation activity of 2933 mA mg<sup>-1</sup><sub>Ni</sub> at 0.55 V; with an onset potential of 0.32 V vs. Ag/AgCl. Chronoamperometry curves of NiCr catalysts show stability over 2000 s in oxidizing urea. A lower charge-transfer resistance of 3.3 Ω cm<sup>2</sup> at 0.40 V was calculated on Ni<sub>60</sub>Cr<sub>40</sub>/C compared to that of Ni/C (13 Ω cm<sup>2</sup>). The exceptionally high mass activity of Ni<sub>60</sub>Cr<sub>40</sub>/C is attributed to improved charge-transfer kinetics, enhanced surface coverage of Ni(II)/Ni(III) redox center, better dispersion of Ni nuclei and a low-Tafel slope.

## 1. Introduction

Growing demands for energy and global warming concerns inspire the development of renewable abundant energy sources. Direct urea fuel cells (DUFCS) are regarded as a clean energy conversion device. DUFCS have recently gained significant attention because urea is used as an alternative fuel to hydrogen, which mitigates problems associated with hydrogen production, storage, and transportation.<sup>[1–3]</sup> However, the power density of DUFCS is lower compared to polymer electrolyte membrane fuel cells (PEMFC), due to the sluggish urea oxidation kinetics at the anode. Urea oxidation on Ni-based catalysts was first reported by G. G. Botte's group in an alkaline solution.<sup>[4]</sup> They proposed a direct mechanism of urea oxidation on Ni, where a nickel oxyhydroxide (NiOOH) intermediate initiates urea oxidation in a sequence of electrochemical steps. Density functional theory calculation suggests an indirect path of urea oxidation, where urea reacts with NiOOH to form its final

product in a chemical step.<sup>[5]</sup> Thereafter, the NiOOH intermediate was probed by *in-situ* surface-enhanced Raman (SER) spectroscopy<sup>[6–8]</sup> and *in-situ* X-ray diffraction (XRD).<sup>[9]</sup> To further improve urea oxidation on Ni catalysts, a variety of binary and ternary Ni-based catalysts with enhanced urea oxidation, such as Ni-Rh<sup>[10]</sup>, Ni-Co<sup>[11,12]</sup>, Ni-Zn-Co<sup>[13]</sup>, Ni/WC<sup>[14]</sup>, and Ni/Sn<sup>[15]</sup> were reported. Most of the catalysts used for urea oxidation were prepared by an electro-deposition method, where the yield is limited<sup>[4,6,12,16]</sup>. NiCo<sub>2</sub>O<sub>4</sub><sup>[17]</sup>, Ni<sub>1.5</sub>Mn<sub>1.5</sub>O<sub>4</sub><sup>[18]</sup>, and LaNiO<sub>3</sub><sup>[19]</sup> with improved performance towards urea oxidation prepared by a chemical synthesis method were recently reported. The mechanism on these catalysts is similar to that of Ni.<sup>[6,16]</sup> Xu *et al.* critically reviewed various aspects of urea oxidation on a variety of Ni surfaces.<sup>[20]</sup> Electrochemical impedance spectroscopy investigation of urea oxidation on Ni suggests both a direct and an indirect mechanism path.<sup>[21]</sup> To date, Ni-based catalysts remain the state-of-the-art for the urea oxidation reaction in alkaline electrolyte.

A NiCr catalyst was recently used in the anode of an alkaline polymer electrolyte fuel cell (APEFC) to improve cell performance.<sup>[22]</sup> It was suggested that Cr helps modify the electronic structure of the d-band by weakening the Ni-O interaction.<sup>[22]</sup> The NiCr/C catalyst also shows excellent tolerance towards quaternary ammonium salts in APMFCs.<sup>[23]</sup> The enhanced methanol oxidation<sup>[24]</sup> and hydrogen evolution<sup>[23]</sup> activities of bimetallic NiCr catalysts in the alkaline medium were reported.

In this article, urea oxidation on NiCr/C catalysts is reported for the first time. The rigorous chemical and electrochemical analysis of NiCr ratios were carried out in order to identify the most active composition of this catalyst. The highest urea oxidation activity of Ni<sub>60</sub>Cr<sub>40</sub>/C catalysts is correlated with the charge-transfer kinetics, particle dispersion, and surface coverage of Ni(II)/Ni(III) redox using a broad range of analytical methods.

## 2. Results and Discussion

The chemical composition of the NiCr catalysts was verified by inductively coupled plasma-optical emission spectrometry (ICP-OES) on the acid dissolved sample and is in good agreement (less than 1%) with the nominal sample composition expected from the reactant ratio (Table S1).

[a] Dr. Ramesh Kumar Singh  
Department of Chemical Sciences  
Ariel University  
Ariel-40700, Israel

[b] Prof. Alex Schechter  
Department of Chemical Sciences  
Ariel University  
Ariel-40700, Israel  
E-mail: salex@ariel.ac.il

## FULL PAPER

WILEY-VCH

X-ray diffraction (XRD) patterns of NiCr/C powder are shown in Figure 1. For comparison, Ni/C and Cr/C XRD patterns are also included in the same figure. The peak at  $25^\circ$  is ascribed to the Vulcan XC-72 carbon-support. The peak observed at  $33.7^\circ$  is assigned to  $\text{Ni(OH)}_2$ , the peak at  $44^\circ$  arises from  $\text{Ni(101)}$  which indicates the formation of metallic Ni, and the peak at  $60.2^\circ$  is attributed to the hexagonal structure of Ni.<sup>[11]</sup> With the incorporation of Cr, the XRD peaks' intensity decreases sharply and almost disappear above 40 at.% Cr. Pure Cr depicts almost no crystalline peaks. Moreover, Cr peaks are completely missing from the XRD pattern. It thus appears that Cr increases the amorphization of NiCr particles with no direct evidence of NiCr alloy formation. It is therefore concluded that chromium controls the Ni crystallite growth while promoting  $\text{Ni(OH)}_2$  formation up to 40 at.% Cr. Above 40 at.% Cr, the  $\text{Ni(101)}$  peak is apparent. The crystallite size estimated from the peak broadening of  $\text{Ni(101)}$  and shown in Table S2. The presence of Ni and Cr is verified from the ICP-OES and scanning electron microscopy (SEM) elemental mapping is shown in the next section.

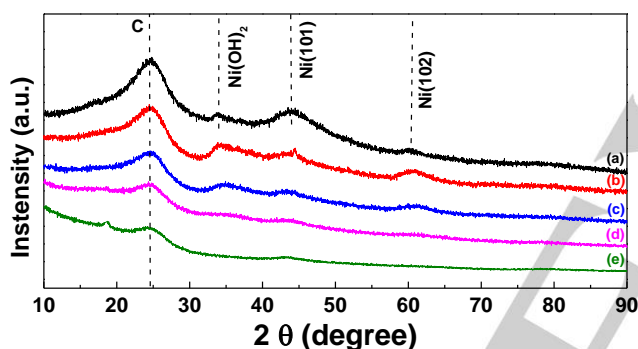


**Figure 1.** X-ray diffraction patterns of Ni/C (a),  $\text{Ni}_{90}\text{Cr}_{20}/\text{C}$  (b),  $\text{Ni}_{60}\text{Cr}_{40}/\text{C}$  (c),  $\text{Ni}_{40}\text{Cr}_{60}/\text{C}$  (d), and Cr/C (e).

Figure 2 presents a typical scanning electron microscopy (SEM) image of a carbon-supported  $\text{Ni}_{60}\text{Cr}_{40}$  catalyst. The morphology of the catalysts is shown in Fig. 2(a) and the corresponding energy dispersive spectroscopic (EDS) analysis of the encircled region of Fig. 2(a) is shown in Fig. 2(b).

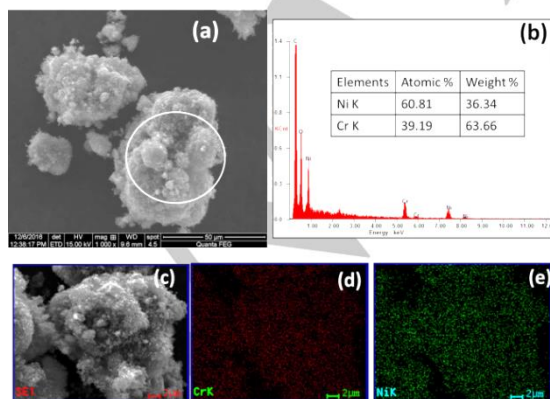


**Figure 2.** SEM image of  $\text{Ni}_{60}\text{Cr}_{40}/\text{C}$  (a), EDS of encircled region (b), SEM image of  $\text{Ni}_{60}\text{Cr}_{40}/\text{C}$  where mapping was performed (c), elemental mapping of Cr (d) and Ni (e).

A selected area SEM image is shown in Fig. 2(c) and the corresponding elemental mapping distributions of Cr and Ni are shown in Fig. 2(d) and (e), respectively, which could indicate the formation of segregated phases of Ni and Cr. Atomic percentages of Ni and Cr obtained from EDS are in good agreement with ICP-OES results.

Overlaid steady state cyclic voltammograms (CVs) of NiCr/C catalysts are shown in Fig. 3. CVs of Ni/C and Cr/C are included for comparison. The CVs show the typical redox feature of Ni as reported in the literature.<sup>[4,6,16]</sup> A featureless voltammogram of Cr/C suggests that it is electrochemically inactive. The anodic peak at  $\sim 0.38$  V is ascribed to oxidation of  $\text{Ni(II)(OH)}_2/\text{Ni(III)OOH}$  and the cathodic peak is attributed to the reversible reduction of  $\text{Ni(III)OOH}$  to  $\text{Ni(II)(OH)}_2$ . Electrochemical parameters from Fig. 3 are given in Table S3. NiCr/C catalysts show a shift in redox peaks to the negative potentials.

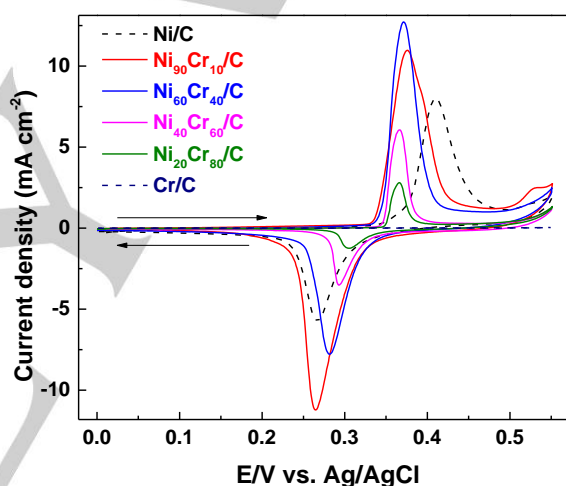


**Figure 3.** Cyclic voltammograms of NiCr/C catalysts in  $\text{N}_2$ -saturated 1 M KOH solution at a scan rate of  $10 \text{ mV s}^{-1}$ .

This shift is assigned to the lower redox potential of  $\text{Cr(II)/Cr(III)}$  couple compared to that of  $\text{Ni(II)/Ni(III)}$ , which may shift the overall redox potential of NiCr compared to that of bare Ni. An increase in the anodic peak current is observed with the increase in Cr content up to 40%. Above 40%, the peak current decreases gradually with the further increase in Cr content to 80%. The redox peak separation potential decreases gradually from 140 to 60 mV with the increase in Cr content (Table S3). An observed peak separation of only 60 mV is seen in 80% Cr, which suggests high reversibility of  $\text{Ni(II)/Ni(III)}$  redox. This redox peak separation is close to the theoretical reversible mixed-diffusion controlled process (59 mV for single electron transfer).<sup>[25]</sup> The electrochemical active surface area (ECSA) is calculated from integration of the charge under the redox peaks using a constant of  $514 \mu\text{C cm}^{-2}$  for Ni surfaces.<sup>[26]</sup> A higher ECSA of  $285 \text{ m}^2 \text{ g}^{-1}_{\text{Ni}}$  is observed in  $\text{Ni}_{60}\text{Cr}_{40}/\text{C}$  compared to  $123 \text{ m}^2 \text{ g}^{-1}_{\text{Ni}}$  of

## FULL PAPER

WILEY-VCH

Ni/C supports better dispersion of smaller Ni nuclei. Thus, the sharp redox features and small peak separation observed on NiCr electrodes point to better charge-transfer kinetics.

The urea oxidation activity of NiCr/C catalysts was measured in 0.33 M urea and 1 M KOH (Fig. 4(a)) and the CVs of Ni/C and Cr/C are included for comparison. In the presence of urea, the anodic current sharply increases in accordance with urea oxidation facilitated by Ni(III) formation (Fig. 3). The oxidation onset potential exactly overlaps that of Ni in KOH solution, suggesting that the reaction is governed by the Ni(II)/Ni(III) redox (Fig. S1). The cathodic peak, assigned to the reduction of NiOOH which was not chemically reduced by urea, serves as an indication that the chemical step (discussed in the next section) is slower than NiOOH formation. At a slow scan rate of  $1 \text{ mV s}^{-1}$ , the cathodic peak current is minute, resulting from an almost complete urea reduction of NiOOH as well as competitive adsorption of hydroxide and urea to the remaining Ni(III) sites. However, the cathodic charge on Ni/C (1 mC) is significantly lower in the presence of urea compared to the cathodic charge in a urea free solution (5.5 mC) of the same electrode and suggests that most of the generated NiOOH react with urea. As seen from Fig. 4(a), Cr/C displays very low currents suggests that it is inactive towards urea oxidation. Electrochemical parameters derived from Fig. 4(a) are listed in Table S4. With the increase in Cr content, a decrease in onset potential is observed up to 40% Cr, and it increases gradually with the increase in Cr content above 40% (Fig. 4(b) and Table S4). A significantly low onset potential of 0.32 V is observed with 40% Cr in NiCr catalysts (Fig. 4(b)). This value is among the lowest reported compared with 0.29 V<sup>[18]</sup>, 0.34 V<sup>[15]</sup>, and 0.35 V<sup>[21]</sup> under similar conditions. Fig. 4(c) displays current densities at selected potentials of 0.40, 0.45, 0.50 and 0.55 V as a function of atomic Cr %, which shows a volcano shape behavior. A similar trend in current density is seen at all potentials, with the highest current at 0.55 V.

The highest mass activity of  $2933 \text{ mA mg}^{-1}_{\text{Ni}}$  at 0.55 V was calculated for Ni<sub>60</sub>Cr<sub>40</sub>/C and is 3.6-fold larger than Ni ( $800 \text{ mA mg}^{-1}_{\text{Ni}}$ ). Ni<sub>1.5</sub>Mn<sub>1.5</sub>O<sub>4</sub><sup>[18]</sup> was recently reported to exhibit enhanced activity towards urea oxidation, where the maximum current of  $7 \text{ mA cm}^{-2}$  at 0.50 V is observed compared to  $65 \text{ mA cm}^{-2}$  at 0.50 V in Ni<sub>60</sub>Cr<sub>40</sub>/C under identical conditions. A fivefold increase in mass activity was observed with Ni<sub>60</sub>Cr<sub>40</sub>/C compared to LaNiO<sub>3</sub><sup>[19]</sup> ( $371 \text{ mA mg}_{\text{oxide}}^{-1}$ ) in 0.33 M urea and 1 M KOH solution.

Tafel slopes of NiCr/C catalysts in the presence of urea are given in Table 1. A Tafel slope of  $16 \text{ mV decade}^{-1}$  was observed on Ni<sub>60</sub>Cr<sub>40</sub>/C, which is lower than that of Ni/C ( $30 \text{ mV decade}^{-1}$ ), suggesting a sharp increase in the current of NiCr catalysts

compared to that of Ni. The similar Tafel slope of  $28 \text{ mV decade}^{-1}$  was reported on Ni film.<sup>[16]</sup> The addition of Cr thus decreases the Tafel slope by a factor of 2 on Ni<sub>60</sub>Cr<sub>40</sub>/C.

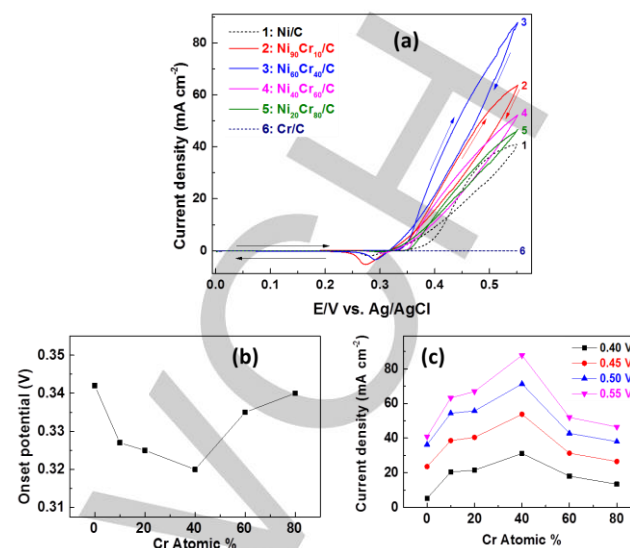


**Figure 4.** Cyclic voltammograms of NiCr/C catalysts in 0.33 M urea and 1 M KOH at a scan rate of  $10 \text{ mV s}^{-1}$  (a), onset potential (b), and current density at potentials of 0.40, 0.45, 0.50 and 0.55 V (c) as a function of Cr atomic %.

**Table 1.** Tafel slopes of various NiCr/C catalysts calculated from the voltammograms in 0.33 M urea/1M KOH solution at a scan rate of  $10 \text{ mV s}^{-1}$ .

Catalysts	Tafel Slope ( $\text{mV decade}^{-1}$ )
Ni/C	30
Ni <sub>90</sub> Cr <sub>10</sub> /C	17
Ni <sub>60</sub> Cr <sub>40</sub> /C	16
Ni <sub>40</sub> Cr <sub>60</sub> /C	15
Ni <sub>20</sub> Cr <sub>80</sub> /C	14

CVs of Ni<sub>60</sub>Cr<sub>40</sub>/C were recorded at various scan rates with and without urea in 1 M KOH electrolyte (Fig. 5). In light of the high activity of the Ni<sub>60</sub>Cr<sub>40</sub>/C electrode, it was selected for this analysis. Fig. 5(a) shows CVs recorded at various scan rates in 1 M KOH solution. Although the Ni(II)/Ni(III) peak current increases, the anodic and cathodic peak potentials do not change much with the scan rate ( $\nu$ ), in line with a redox reversible reaction. A plot of cathodic current density as a function of scan rate ( $\nu$ ) shows linear behavior and indicates a surface confined redox (inset to Fig. 5(a)). This behavior is in line with that reported by R. Zhang *et al.* where the peak current density ( $I_p$ ) proportional to the scan rate below  $0.1 \text{ V s}^{-1}$  is attributed to surface-confined redox and above  $0.1 \text{ V s}^{-1}$ , it becomes proportional to the square root of the scan rate of a dominant diffusion process.<sup>[27]</sup> The surface coverage of Ni(II)/Ni(III) redox is estimated from Eqn. (1).<sup>[27]</sup>

$$I_p = n^2 F^2 \nu A \Gamma / (4RT) \quad (1)$$

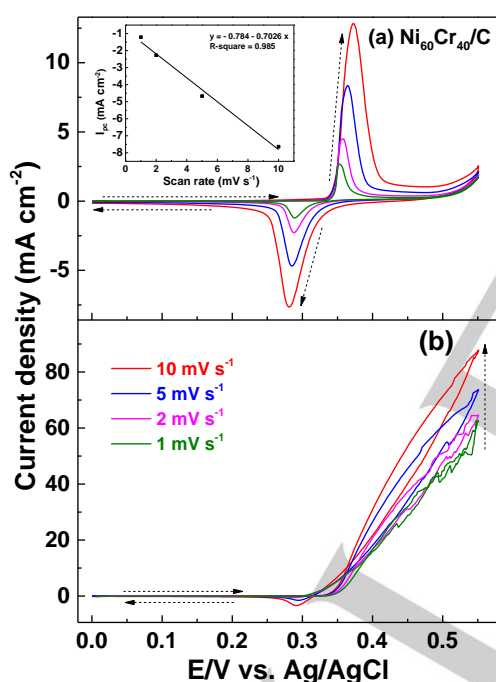
## FULL PAPER

WILEY-VCH

Where  $I_p$ : peak current,  $n$ : number of electrons transferred,  $F$ : Faraday constant,  $\nu$ : scan rate,  $A$ : geometrical electrode area,  $\Gamma$ : surface coverage of Ni(II)/Ni(III) redox,  $R$ : universal gas constant, and  $T$ : temperature.

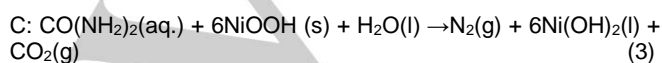
From the slope of the  $I_{pc}$  vs scan rate plot, the surface coverage of the Ni(II)/Ni(III) redox sites was estimated to be  $7.5 \times 10^{-7}$  mole  $\text{cm}^{-2}$ , which is higher than Ni/C ( $5.0 \times 10^{-7}$  mole  $\text{cm}^{-2}$ ) and in agreement with the activity and better dispersion of the Ni active sites.

Fig. 5(b) shows voltammograms of  $\text{Ni}_{60}\text{Cr}_{40}/\text{C}$  as a function of scan rate in a urea solution. An increase in anodic current density is observed with a scan rate at a potential above 0.45 V. With the increase in scan rate from 1 to 10  $\text{mV s}^{-1}$ , the current at 0.55 V changes by 55%, from 55 to 85  $\text{mA cm}^{-2}$ . An increase in the cathodic peak current with the scan rate is moderate. This is attributed to the sluggish urea oxidation reaction rather than the electro-oxidation of  $\text{Ni}(\text{OH})_2$  to  $\text{NiOOH}$  (Eqn. 3).



**Figure 5.** CVs of  $\text{Ni}_{60}\text{Cr}_{40}/\text{C}$  in  $\text{N}_2$ -saturated 1 M KOH (a) and 0.33 M urea/1 M KOH at various scan rates; inset to Fig. 5(a) shows a plot of cathodic peak current density ( $I_{pc}$ ) as a function of scan rate.

The fact that the cathodic current is low compared to the Ni redox current is an indication of a slower chemical step (Eqn. 3) than  $\text{NiOOH}$  formation (Eqn. 2).



Where E: electrochemical step and C: chemical step, as reported in the literature.<sup>[6]</sup> The oxidation products of urea are  $\text{N}_2$  and  $\text{CO}_2$ .

A similar increase in cathodic current with scan rate was reported by Bryan K. Boggs *et al.* in the presence of urea.<sup>[4]</sup> The fact that the increase in the urea oxidation current is not proportional to the scan rate, contrary to 1 M KOH, further supports the claim that the urea oxidation reaction is not purely electrochemical and that it proceeds *via* an electrochemical-chemical (EC) mechanism.<sup>[6]</sup> It is important to note that no change in the voltammogram was observed above 0.45 V, indicating that no water oxidation takes place.

Chronoamperometric experiments of NiCr catalysts were carried out to evaluate the stability of catalysts for urea oxidation (Fig. 6). A stable current persists during a measurement time of 2000s in oxidizing urea. The higher current observed with  $\text{Ni}_{60}\text{Cr}_{40}/\text{C}$ , with respect to other NiCr and Ni electrodes, is in line with the voltammetric results (Fig. 4(a)). The noise in the chronoamperometric curves is due to the formation of  $\text{N}_2$  and  $\text{CO}_2$  bubbles on the electrode surface with time.

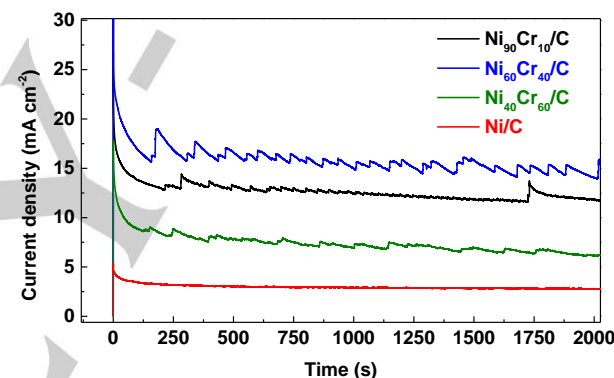


**Figure 6.** Chronoamperometry plot of NiCr/C catalysts in 0.33 M urea/1 M KOH at 0.40 V vs.  $\text{Ag}/\text{AgCl}$ .

Electrochemical impedance spectroscopy was performed to further probe the urea oxidation reaction on NiCr/C catalysts. Typical Nyquist plots of NiCr/C catalysts at potentials of 350 and 400 mV are shown in Figs. 7(a) and (b), respectively. The charge-transfer resistance proportional to the semi-circle diameter decreases by one order of magnitude with the increase in potential from 350 to 400 mV. The diameter of the semicircle gives charge-transfer resistance ( $R_{ct}$ ). The  $R_{ct}$  of NiCr catalysts is given in Table S5. At 350 mV, the charge-transfer resistance of Ni/C is  $95 \Omega\text{-cm}^2$  and decreases sharply to  $13 \Omega\text{-cm}^2$  at 400 mV. The lowest charge-transfer resistance of only 6 and  $3.3 \Omega\text{-cm}^2$  at the potential of 350 and 400 mV, respectively, was calculated on  $\text{Ni}_{60}\text{Cr}_{40}/\text{C}$  (Table S5). Thus, the  $\text{Ni}_{60}\text{Cr}_{40}/\text{C}$  catalyst exhibits excellent charge-transfer kinetics towards urea oxidation.

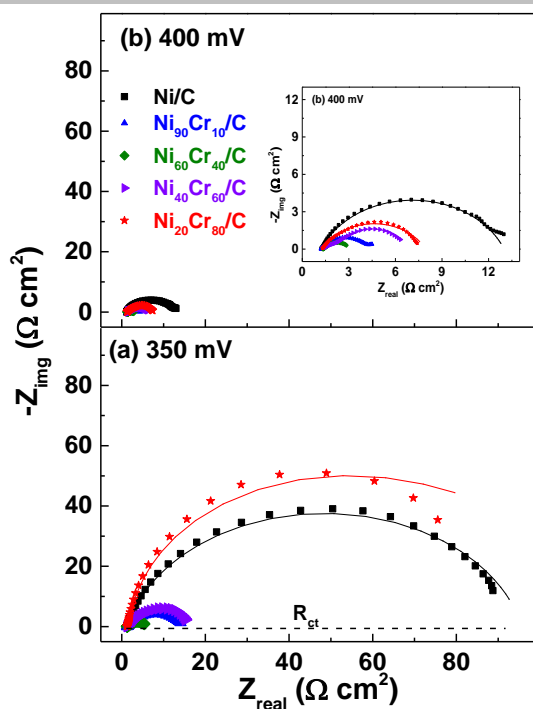


**Figure 7.** Nyquist plots of NiCr/C catalysts at 350 mV (a) and 400 mV (b) in 0.33 M urea and 1 M KOH solution from 10 kHz to 50 mHz frequency range. Inset to Fig. 7(b) shows the magnified view. The solid lines show the fitted data.

A plot of charge-transfer resistance as a function of Cr atomic % at potentials of 350 and 400 mV is shown in Fig. 8. The enlarged region of the plot is shown in the inset to reflect differences in charge-transfer resistance. The choice of these potentials reflects the sharpest change in charge-transfer resistance, above these potentials the differences among the catalyst resistance are minute. At 350 mV, the resistance decreased drastically from 95 to 12  $\Omega \text{ cm}^2$  with an increase in Cr content from 0 to 10%, where the lowest resistance of 6  $\Omega \text{ cm}^2$  was observed with 40% Cr. Above 40% Cr, an increase in charge-transfer resistance was observed at both potentials. At 400 mV, the resistance does not change sharply with Cr content, and the lowest resistance of 3.3  $\Omega \text{ cm}^2$  was observed at 40% Cr. The charge-transfer corresponds to the current recorded in the voltammetric results (Fig. 4(a)). The metallic chromium itself has high charge-transfer resistance of 7890  $\Omega \text{ cm}^2$  at 400 mV, which means that it is inactive in urea oxidation. Ni(OH)<sub>2</sub>/NiOOH is thus the active part in Ni:Cr. We, therefore, believe that the mechanism of urea oxidation with NiCr/C catalysts is similar to that reported by Botte's group, where NiOOH mediates the preferential oxidation of urea to its products.<sup>[5,6,16]</sup> In addition, adsorption of urea on Ni surface is facilitated through urea carbon center based on the theoretical calculation by Daramola et al.<sup>[5]</sup> As reported by Lu *et al.* the modification of Cr oxide on Ni(111) surface decreases the density of state of the *d*-band by the weakening of the Ni-O bond which gives the convincing

evidence for the tuning of the electronic property of Ni.<sup>[22]</sup> We believe that the electronic effect of Cr on Ni surfaces is seen from the volcano shape of the onset potential plot (Fig. 4(b)).

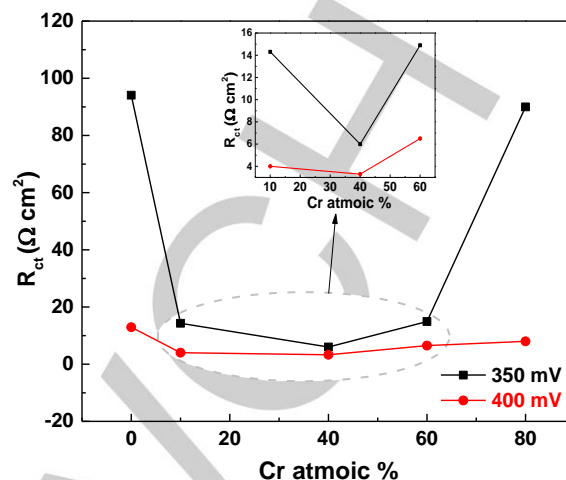


**Figure 8.** The plot of charge-transfer resistance as a function of Cr at. % at applied potentials of 350 and 400 mV. The inset shows the magnified view of encircled region.

### 3. Conclusions

Various compositions of NiCr/C were synthesized by direct borohydride reduction at room temperature. The composition of NiCr catalysts was studied and it was found that 40% Cr, 60% Ni exhibits the highest urea oxidation activity of 2933  $\text{mA mg}^{-1}_{\text{Ni}}$  at a potential of 0.55 V with an onset potential of 0.32 V vs. Ag/AgCl. This urea oxidation activity value is 3.6 times higher than for Ni/C. However, bare Cr is electrochemically inactive towards urea oxidation. With the increase in Cr content, the amorphous phase of the catalyst was observed from the XRD patterns and the reversibility of Ni(II)/Ni(III) redox increases. Cr seems to have the dispersion effect to Ni nuclei. The lowest charge-transfer resistance of Ni<sub>60</sub>Cr<sub>40</sub>/C reflects improved urea charge-transfer kinetics. The exceptionally high mass activity of Ni<sub>60</sub>Cr<sub>40</sub>/C is attributed to the improved charge-transfer kinetics, better dispersion of Ni nuclei, high surface coverage of Ni(II)/Ni(III) redox center and low Tafel slope.

### Experimental Section

#### Materials

Chromium (III) chloride hexahydrate ( $\text{CrCl}_3 \cdot 6\text{H}_2\text{O}$ , 98%) and sodium borohydride ( $\text{NaBH}_4$ , 98%) from Acros Organics; urea ( $\text{NH}_2\text{CONH}_2$ ; 99.0–100.5%) from Alfa Aesar; nickel (II) nitrate hexahydrate ( $\text{Ni}(\text{NO}_3)_2 \cdot 6\text{H}_2\text{O}$ ; 99.99%) from Strem Chemicals; Nafion (5 wt% solution in aliphatic alcohol) from ion power; potassium hydroxide (KOH), and isopropyl alcohol from Frutarom Ltd., Israel were used as received. High purity (18.2 M $\Omega$ ) de-ionized water (DIW) was used for the synthesis.

### Synthesis of Various Compositions of NiCr/C

The experimental conditions for catalyst synthesis are presented in Table S6. For the typical catalyst synthesis, salts of Ni ( $\text{Ni}(\text{NO}_3)_2 \cdot 6\text{H}_2\text{O}$ ) and Cr ( $\text{CrCl}_3 \cdot 6\text{H}_2\text{O}$ ) were mixed in the required atomic ratio in an argon-purged solution. The required amount (160 mg) of Vulcan XC-72R carbon was added to maintain a 20 wt% loading of the catalyst on the carbon support and the solution was stirred for another 1 h. The resultant solution was reduced by drop-wise addition of freshly prepared 4 wt%  $\text{NaBH}_4$  while stirring. After reduction, the black solution was centrifuged at 3500 rpm for 10 min to collect the solid product. The black powder was washed 3 times with DIW, re-dispersed in isopropyl alcohol and dried at 70°C overnight. Bare Ni/C was synthesized by a similar procedure, without the addition of chromium salt.

### Electrode Fabrication

The glassy carbon disk electrodes were coated by catalyst ink. For the typical preparation of catalyst ink: 25 mg catalyst, 2 mL isopropyl alcohol (IPA), 1 mL water and 100  $\mu\text{L}$  Nafion were sonicated for 30 min to form a homogeneous suspension of the catalysts ink. Then, 6  $\mu\text{L}$  of catalyst suspension was drop-cast on the glassy carbon disk electrode to maintain a metal loading of  $\sim 50 \mu\text{g cm}^{-2}$ .

### Instrumentation

The metal loading and atomic composition of NiCr/C samples were verified by a Varian 710-ES Inductively Coupled Plasma-Optical Emission Spectrometer (ICP-OES). The NiCr samples were further analyzed by X-ray diffraction (XRD) using the Rigaku SmartLab X-ray diffractometer employing Bragg-Brentano optics (BB/PSA). The X-ray generator was operated at 40 kV and 30 mA with Cu-K $\alpha$  radiation ( $\lambda = 1.54 \text{ \AA}$ ). Scanning electron microscopy (SEM) measurement was performed on an ESEM Quanta FEG 250 system. The images were collected using secondary electron imaging (SEI) and backscattered electron (BE) detectors equipped with energy dispersive X-ray spectroscopy (EDS) from AMETEK, FEI Quanta 200/400. Electrochemical studies were performed in three electrode configurations, with a Biologic potentiostat (VSP, Biologic Science Instruments). The catalyzed glassy carbon disk electrode served as a working electrode (from Pine Instruments), Ag/AgCl as a reference electrode (Metrohm) and Pt wire as a counter electrode. The area of the glassy carbon disk electrode was 0.196  $\text{cm}^2$ . Electrochemical impedance spectroscopy (EIS) measurements were performed using an AC amplitude of 10 mV in the frequency range of 10 kHz to 50 mHz. EIS patterns were fitted by the complex non-linear least square (CNLS) fit using ZsimpWin software from Biologic.

### Acknowledgements

We acknowledge the support of the Israeli *Fuel Choices Initiative* and the Israel Science Foundation (ISF) for partially supporting the research work through the Israel National Research Center for Electrochemical Propulsion (INREP) and I-CORE Program (number 2797/11).

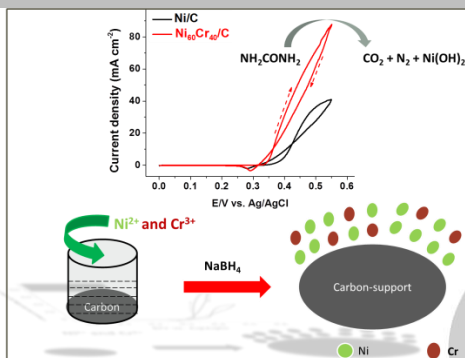
**Keywords:** NiCr/C • urea oxidation • surface redox • electrochemical impedance spectroscopy • borohydride reduction

### References

- [1] X. Ren, P. Zelenay, S. Thomas, J. Davey, S. Gottesfeld, *J. Power Sources* **2000**, 111–116.
- [2] A. Kowal, M. Li, M. Shao, K. Sasaki, M. B. Vukmirovic, J. Zhang, N. S. Marinkovic, P. Liu, a. I. Frenkel, R. R. Adzic, *Nat. Mater.* **2009**, *8*, 325–330.
- [3] U. B. Demirci, P. Miele, *Energy Environ. Sci.* **2011**, *4*, 3334.
- [4] B. K. Boggs, R. L. King, G. G. Botte, *Chem. Commun. (Camb)*. **2009**, *2009*, 4859–4861.
- [5] D. A. Daramola, D. Singh, G. G. Botte, *J. Phys. Chem. A* **2010**, *114*, 11513–11521.
- [6] V. Vedharathinam, G. G. Botte, *Electrochim. Acta* **2013**, *108*, 660–665.
- [7] J. Desilvestro, *J. Electrochem. Soc.* **1988**, *135*, 885.
- [8] J. Desilvestro, D. a Corrigan, M. J. Weaver, *J. Phys. Chem.* **1986**, *90*, 6408–6411.
- [9] D. Wang, G. G. Botte, *ECSC Electrochem. Lett.* **2014**, *3*, H29–H32.
- [10] R. L. King, G. G. Botte, *J. Power Sources* **2011**, *196*, 9579–9584.
- [11] W. Xu, H. Zhang, G. Li, Z. Wu, *Sci. Rep.* **2014**, *4*, 5863.
- [12] W. Yan, D. Wang, G. G. Botte, *Electrochim. Acta* **2012**, *61*, 25–30.
- [13] W. Yan, D. Wang, G. G. Botte, *Appl. Catal. B Environ.* **2012**, *127*, 221–226.
- [14] L. Wang, M. Li, Z. Huang, Y. Li, S. Qi, C. Yi, B. Yang, *J. Power Sources* **2014**, *264*, 282–289.
- [15] R. K. Singh, P. Subramanian, A. Schechter, *ChemElectroChem* **2017**, DOI 10.1002/celec.201600862.
- [16] V. Vedharathinam, G. G. Botte, *Electrochim. Acta* **2012**, *81*, 292–300.
- [17] R. Ding, L. Qi, M. Jia, H. Wang, *Nanoscale* **2014**, *6*, 1369–76.
- [18] S. Periyasamy, P. Subramanian, E. Levi, D. Aurbach, A. Gedanken, A. Schechter, *ACS Appl. Mater. Interfaces* **2016**, *8*, 12176–12185.
- [19] R. P. Forslund, J. T. Mefford, W. G. Hardin, C. T. Alexander, K. P. Johnston, K. J. Stevenson, *ACS Catal.* **2016**, *6*, 5044–5051.
- [20] W. Xu, Z. Wu, S. Tao, *Energy Technol.* **2016**, *3800*, 1329–1337.
- [21] F. Guo, K. Ye, M. Du, X. Huang, K. Cheng, G. Wang, D. Cao, *Electrochim. Acta* **2016**, *210*, 474–482.
- [22] S. Lu, J. Pan, A. Huang, L. Zhuang, J. Lu, *Proc. Natl. Acad. Sci. U. S. A.* **2008**, *105*, 20611–20614.
- [23] M. K. Bates, Q. Jia, N. Ramaswamy, R. J. Allen, S. Mukerjee, *J. Phys. Chem. C* **2015**, *119*, 5467–5477.
- [24] Y. Gu, J. Luo, Y. Liu, H. Yang, R. Ouyang, Y. Miao, *J. Nanosci. Nanotechnol.* **2015**, *15*, 3743–3749.
- [25] J. Wang, *Analytical Electrochemistry*, John Wiley & Sons, **2006**.
- [26] M. Grdeń, M. Alsabet, G. Jerkiewicz, *ACS Appl. Mater. Interfaces* **2012**, *4*, 3012–3021.
- [27] R. Zhang, W. Zhang, L. Gao, J. Zhang, P. Li, W. Wang, R. Li, *Appl. Catal. A Gen.* **2013**, *466*, 264–271.

## FULL PAPER

Enhanced urea oxidation activity of  $\text{Ni}_{60}\text{Cr}_{40}/\text{C}$  is attributed to improved charge-transfer kinetics, better dispersion of Ni nuclei, high surface coverage of Ni(II)/Ni(III) redox center and low Tafel slope.



Ramesh Kumar Singh, Alex Schechter\*

**Electroactivity of Urea Oxidation on NiCr Catalysts in Alkaline Electrolyte**